Catalysis Science & Technology

Accepted Manuscript

This article can be cited before page numbers have been issued, to do this please use: Y. Huang, Z. Liu, G. Gao, Q. Xiao, W. N. Martens, A. Du, S. Sarina, C. Guo and H. Zhu, *Catal. Sci. Technol.*, 2017, DOI: 10.1039/C7CY02291C.

ROYAL SOCIETY OF CHEMISTRY

rsc.li/catalysis

View Article Online
DOI: 10.1039/C7CY02291C

Journal Name

ARTICLE

Visible light driven selective hydrogenation of unsaturated aromatics in aqueous solution by direct photocatalysis of Au nanoparticle

Received 00th January 20xx,
Accepted 00th January 20xx

DOI: 10.1039/x0xx00000x

www.rsc.org/

Yiming Huang,[a] Zhe Liu,[a] Guoping Gao,[a] Qi Xiao,[a, b] Wayde Martens,[a] Aijun Du,[a] Sarina Sarina,*[a] Cheng Guo,[c] and Huaiyong Zhu[a]

Abstract: Selective hydrogenation of various chemical bonds, C=C, C≡C, C=O, N=O and C=N are efficiently driven by visible light over supported gold nanoparticle (AuNP) photocatalyst under mild reaction conditions. The reaction system exhibits high substituent tolerance and tunable selectivity by light wavelength. Density functional theory (DFT) calculation demonstrated a strong chemisorption between reactant molecule and metal resulting in a hybridized orbitals. It is proposed that direct photoexcitation between the hybridized orbitals is the main driving force of the hydrogenation reaction. The hydrogenation pathway is investigated with isotope tracking technique. We reveal the cooperation of water and formic acid (FA) as hydrogen source and its hydrogenation route through Au-H species on the AuNP surface.

Introduction

Photocatalysis using plasmonic metal (Au, Ag, Cu) nanoparticles (NPs) has attracted much attention because it directly utilize solar power and usually associate with mild reaction conditions.[1-8] The NPs of these metal strongly absorb visible light via localized surface plasmson resonance (LSPR) effect which is the light-induced collective oscillation of the metal conduction electrons, established when the incident light frequency is resonant with the frequency of metal electron oscillation in response to the restoring force of the positive nuclei, it results in photoexcitation of electrons.[9-11] Chemical transformations can thusly be mediated due to the direct charge excitation within the metal-adsorbed organic molecular system.[12] Linic *et* al proposed the detailed theory that the strong chemisorption between metal NPs and organic reactant leads to the hybridized orbitals. The light irradiation can direct excite electrons between those orbitals to trigger chemical transformations.[13,14]

The selective hydrogenation of unsaturated organics is a fundamental reaction in organic synthesis that traditionally attained with the assistance of pressurized hydrogen gas under high pressures, and elevated reaction temperatures (over 100°C).[15] Elevated temperature in traditional hydrogenation may accelerate undesired side reactions, such as hydrogenation of the aromatic rings of the reactants, wasting the reduction agent resulting in poor economic viability.[16,17] In respect to moderate reaction condition, various homogeneous or heterogeneous transition metal based catalysts including gold, nickel, ruthenium, cobalt, copper or palladium are widely employed in the hydrogenation of unsaturated bonds of C=C, C≡C, C=O, N=O and C=N toward benign processes.[18-21] Yet, challenges remain in energy efficiency, product selectivity and catalyst recyclability.[22] Thus, the hydrogenation reactions can be greatly promoted by visible light driven mild photocatalysis. Meanwhile, the high corrosivity of hydrogen gas at high pressure and temperature causes hydrogen embrittlement of pressurized metal reactors resulting high safety risks.[23,24] In contrast, with other reducing agent such as formic acid (FA), the necessity of high pressure vessels as well as corresponding risks can be avoided.[25] FA is an environmentally green liquid reducing agent readily produced from biomass, being a convenient hydrogen donor, it only generates carbon dioxide and water as oxidized products.[26] Commercially supplied FA is always an aqueous solution. In organic synthesis, however, water is not a widely used solvent despite its low cost and low environmental toxicity.[27,28] Hence, there have been limited reports involving aqueous solution of FA in organic hydrogenation reactions to the best of our knowledge.[29-31]

In this work, we developed an environmental friendly selective hydrogenation system for unsaturated aromatics, the reaction is driven by a renewable energy source visible light irradiation, FA aqueous solution is employed as a green hydrogen source and the reaction is taken place in water solvent. The supported AuNP photocatalyst is prepared by impregnation-reduction method. Five representative types of

[a] School of Chemistry, Physics and Mechanical, Faculty of Science and Technology, Queensland University of Technology, Brisbane, Queensland 4001, Australia. E-mail: S.Sarina@qut.edu.au.
[b] Ian Wark Laboratory, Commonwealth Scientific and Industrial Research Organisation, Bayview Ave, Clayton, Victoria 3168, Australia
[c] College of Science, Nanjing University of Technology, Nanjing, Jiangsu 211800, China.

† Footnotes relating to the title and/or authors should appear here.
Electronic Supplementary Information (ESI) available: [details of any supplementary information available should be included here]. See DOI: 10.1039/x0xx00000x

View Article Online
DOI: 10.1039/C7CY02291C

hydrogenation reactions were investigated under mild temperature in aqueous FA solution without other additives. The reaction mechanism is investigated by isotope study where we found water plays more role than solvent but a hydrogen source cooperated with FA.

Results and Discussion

DFT calculation is conducted using nitrobenzene as modelling molecule to simulate the adsorption of reactant onto AuNP surface, as shown in Figure 1a, the possible bonding between nitrobenzene and an isolated Au cluster is 3.836 Å which suggests a low affinity. On the other hand, a strong chemisorption was observed between nitrobenzene molecule and ZrO_2 supported AuNP as indicated in Figure 1b. The nitrobenzene molecule bond with Au through two O-Au bonds with around 2.1 Å bond length, the adsorption energy was calculated to be -0.802 eV. Such strong bonding results in an organic-metal complex on the AuNP surface and hybridization of their orbitals to for bonding and antibonding states. In this study, the HOMO-LUMO gap of gas-phase nitrobenzene molecule is calculated to be 3.25 eV and that of isolated AuNP is 0.36 eV, however the HOMO-LUMO gap for nitrobenzene-Au complexes was found remarkably reduced to be 0.18 eV which is lower than both isolated AuNP and nitrobenzene. Consequently, the direct resonant photoexcitation of electron take place between the hybridized bonding and antibonding states.[13] This direct photoexcitation is the main reason for the enhanced reaction activity under light irradiation.

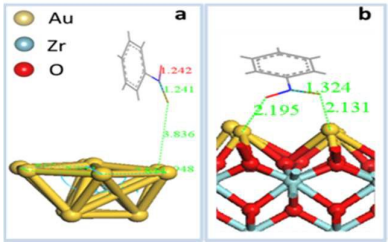

Figure 1. Chemisorption of nitrobenzene onto Au cluster (a) and ZrO2 supported Au NP (b) simulated using DFT methods.

The photocatalytic hydrogenation reaction system was tested with five types of unsaturated aromatics, the catalytic activities of model reactions as well as control reactions, presented with product yields, are shown in Table 1. For nitrobenzene hydrogenation, the reaction under 0.5 W/cm^2 light irradiation results in 98% yield whereas 13% in the dark. Similarly results were observed with hydrogenation of styrene, benzaldehyde, phenylacetylene and benzalaniline. The remarkable difference in the yields between the reactions under irradiation and in the dark demonstrates the contribution of photocatalysis. Such contribution is quantitatively reflected by the 73% decrease of apparent activation energy between light irradiated styrene hydrogenation and that of reaction in dark, 35.3% decrease was observed for the hydrogenation of nitrobenzene (Figure S1). The broad functional group tolerance of the new photocatalytic system is demonstrated in Table 1. The irradiation promotes the hydrogenation with excellent tolerance to various functional groups, especially reducible substituents such as ketones, aldehydes and alkenes.

Table 1. Performance of Au@ZrO2 catalyst for five hydrogenation reactions. The red numbers are the product yield under visible light irradiation, and the black numbers in the parentheses are the product yield for the control reaction in the dark.

Hydrogenation of Aromatic Olefins[a]

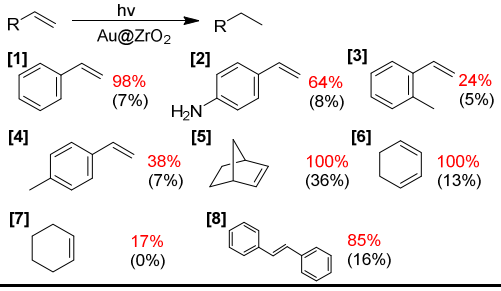

Hydrogenation of Aromatic Nitro-compounds

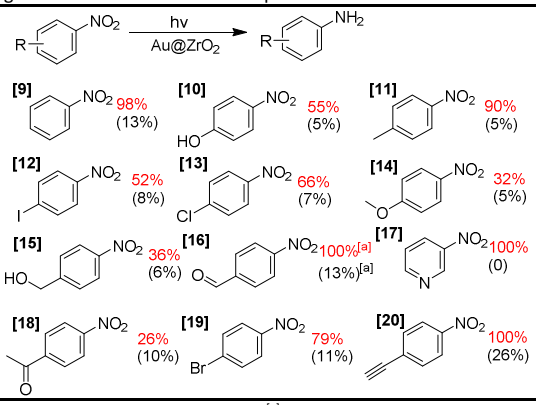

Hydrogenation of Aromatic Aldehydes[a]

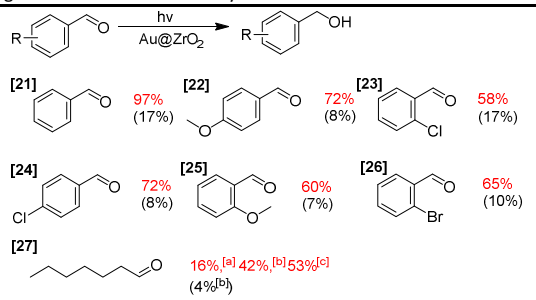

Hydrogenation of Aromatic Alkyne[d]

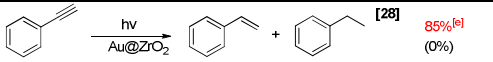

Hydrogenation of Aromatic Imine[a]

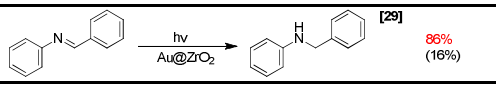

Reaction conditions: 50 mg catalysts, 1 mmol reactant, 2 mL of 85% FA mixed with 2 mL deionized water as solvent, light intensity 0.5 W/cm^2, 40°C, 1 atm argon, reaction time 8 h. [a] reaction time 16 h. [b] 80°C, reaction time 24 h. [c] UV light with peak wavelength at 365 nm, 24 h. [d] 60°C, 16 h. [e] combined yield of both styrene and ethylbenzene. The products were identified by mass spectrometry (MS) and yields were measured by gas chromatography (GC) using external standard.

View Article Online
DOI: 10.1039/C7CY02291C

It is worth noting that FA itself, having a carbonyl group, should be active for the condensation with amines and alkenes at elevated temperatures (over 70 °C).[32] The low operating temperature allows our photocatalytic reaction system to effectively avoid such side reactions and achieving extraordinary chemoselectivity.

Compared to aromatic aldehyde (Table 1, entry 21), we found a poor yield (17%) for aliphatic aldehyde at 40 °C whereas negligible activity was observed in the dark (Table 1, entry 27). The hydrogenation of aliphatic aldehyde demands greater reduction power since the reduction potential of aliphatic aldehydes is generally more negative than that of aromatic aldehydes. For example, the reduction potential of acetaldehyde is -1.7 eV and that of benzaldehyde is -1.36 eV (Table S1). When the hydrogenation of aliphatic aldehyde was conducted under UV irradiation at 40 °C a much higher yield of 53% was achieved. The energy of UV photons is greater than that of visible photons, meaning the UV photons are able to generate photoexcited electrons with higher energies than the ones generated by LSPR absorption of Au NPs in the visible range. These higher energy electrons are capable of reducing compounds with more negative reduction potentials.[33] In addition, when the reaction temperature was raised to 80 °C and the reaction was prolonged to 24 h, the yields for visible light irradiated reaction and reaction in the dark were 42% and 4%, respectively. Therefore, we conclude that AuNPs can combine photonic energy (light) and thermal energy (heat or IR irradiation) because metals have a continuous electron energy level. Above results reveal an important feature that the reduction power of the reported system is tuneable by regulating the irradiation wavelength and reaction temperature.

Table 2. Impact of water/FA ratio on the reductive performance of phenylacetylene hydrogenation

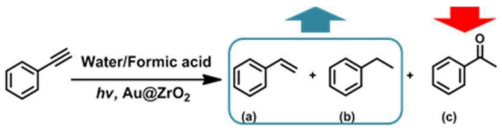

Entry	H_2O/FA (Volume ratio)	Conversion %	Selectivity		
			a	b	c
1	1.5:8.5	100	0	0	100
2	3.5:6.5	100	0	10	90
3	6:4	100	25	59	15
4	8:2	100	22	73	5

Reaction conditions: 50 mg $Au@ZrO_2$ photocatalyst, 0.3 mmol phenylethyne as reactant, formic acid mixed with H_2O as solvent, 0.5 W/cm^2 irradiance, 60 °C, 1 atm argon gas and 16 h.

An unexpected finding is that the ratio of water to FA in the FA aqueous solution has significant impact on the reductive activity of the photocatalytic system. For example, in our reaction system, phenylacetylene was reduced to styrene and ethylbenzene along with side product of acetophenone, which is attributed to the hydration of phenylacetylene in the presence of a hydroxyl group.[34] As shown in Table 2, increasing water/FA ratio can significantly enhance the yields of reductive products, while the production of acetophenone is inhibited. In the cases of benzaldehyde and styrene hydrogenation (Table S2), increasing water ratio can remarkably promote the reaction rate. These results imply a role more than solvent for water. Prior to the mechanism investigation, the $Au@ZrO_2$ photocatalyst was characterized. Figure 2a indicates 3 wt% AuNPs, with a mean size of 7 nm (Figure 2d), are well dispersed on the ZrO_2 surface and predominantly exhibit crystal face (111) (Figure 2b). Light absorption peak of $Au@ZrO_2$ at 520 nm (Figure 2c) is attributed to the LSPR effect of AuNPs as ZrO_2 support exhibits negligible visible light absorption. AuNPs also absorb UV light because electrons of metal can be directly excited by photons from ground state to high energy states.

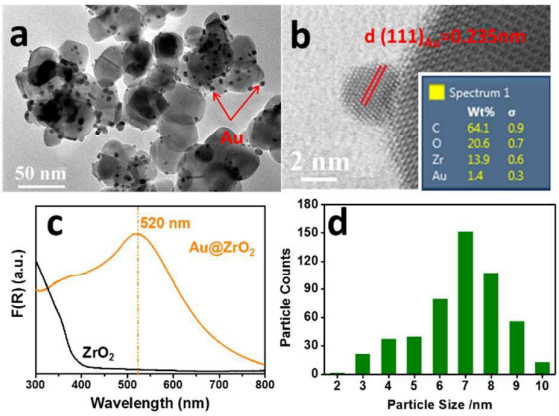

Figure 2. Characterizations of $Au@ZrO_2$ photocatalyst. (a) TEM image and (b) High-resolution TEM image of $Au@ZrO_2$, (c) Diffuse reflectance UV-vis spectra of $Au@ZrO_2$ and ZrO_2 after Kubelka-Munk transformation; (d) Particle size distribution of $Au@ZrO_2$.

To clarify the reaction pathway, isotope tracking was applied by using D_2O and $H_2{}^{18}O$. We found the H-D ratio in the product ethylbenzene was 28% to 72%, which is close to 1:2.5. Such an H-D ratio in the product cannot be rationalized by cation exchange between FA and water (the excessive amount of water in FA solution should causing H-D ratio 1:4 in a typical reaction). Pure water was found no activity in the hydrogenation. Hence, we hypothesis that hydrogen atoms are transferred from water to the reactant in the assistance of FA. The role of water could be overlooked although FA aqueous solution was previously reported as hydrogen donor.[35] Among gaseous products, $C^{18}O_2$ was detected with a ^{16}O:^{18}O ratio approximately 2:1 when $H_2{}^{18}O$ was used. A rational deduction is that FA reacts with $H_2{}^{18}O$ producing an intermediate subsequently provides hydrogen to the styrene hydrogenation and itself is oxidized to $C^{18}O_2$ and H_2O. The possible intermediate is orthoformic acid which has the formula $HC(OH)_3$,[36] being a unstable hydrate has not been isolated to date which consists of one water and one FA molecule.

View Article Online
DOI: 10.1039/C7CY02291C

The proposed complete route is illustrated in Scheme 1. The hydration of FA (step 1,) yields orthoformic acid, which is then oxidized on the surface of AuNPs (step 2), yielding H-Au surface species.[37] The orthoformic acid is oxidized possibly following the same principle as the oxidation of a primary alcohol to carboxylic acid and eventually to carbon dioxide and water.[38]

In the next step, firstly the reactant molecular is adsorbed on the surface of Au nanoparticles following the adsorption model shown in Figure 1b. In order to further verify the chemisorption, taking nitrobenzene adsorbed on Au@ZrO_2 as an example, FTIR was employed to analyse the adsorbed nitrobenzene, the spectrum of adsorbed nitrobenzene shown in Figure S2 shows characteristic peaks from nitrobenzene with a ~8 cm^{-1} shifting, it indicates the existence of the chemisorption that is in agreement with the model from Figure 1b.

Thus, the H-Au surface species are capable of reducing chemisorbed reactant, in styrene's case, two hydrogen atoms are added into the C=C double bond basically following Horiuti-Polanyi Mechanism (step 3 and 4,),[39] the reaction equation as follow:

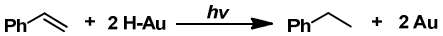

These two reduction steps consume 2 H-Au species and restore the AuNP surface for subsequent catalytic cycles (step 5,). This inference is supported by the fact that the reduction is inhibited when removing these surface species by adding 0.1 equiv. of 2, 2', 6, 6'-tetra-methylpiperidine N-oxyl (TEMPO) to the photocatalytic reaction system, which can abstract hydrogen atoms from the AuNP surface,[40] and found only trace amounts of ethylbenzene in the product.

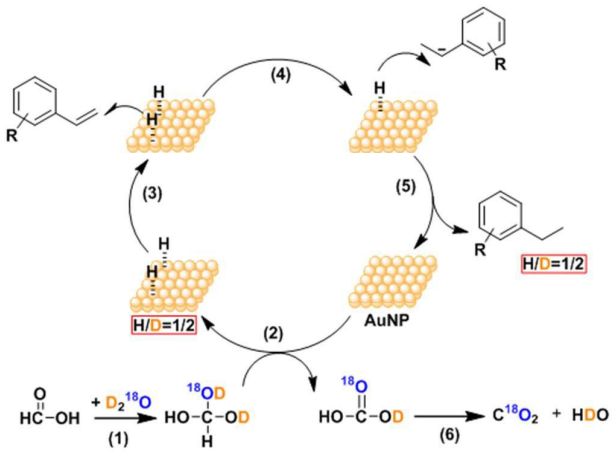

Scheme 1. Mechanism for the photocatalytic hydrogenation of styrene.

The proposed reaction mechanism is supported by step to step isotope study. According to step 1 in Scheme 1, the H-Au (or D-Au) surface species form on the AuNP surface with the H (or D) atoms from the orthoformic acid and the H or D atom should be eventually found in the product ethylbenzene. When D_2O was used, the orthoformic acid formed in the reaction has two D atoms and one H atom available to yield the H-Au surface species (product of step 2). Therefore, the ratio of H to D in the product ethylbenzene should be 1:2, which is very close to our observation mentioned above. Similarly, when $H_2{}^{18}O$ was used, the content of ^{18}O atoms in the product CO_2, is agreed with the experimental observation.

The proposed mechanism is verified with the hydrogenation of nitrobenzene. Similar results were received, shown in Table 3, except pure $^{16}O_2$ was observed in gaseous product suggesting a source differ from $H_2{}^{18}O$. We investigated the compositional evolution of the reaction (Figure 3a). In the first two hours, the nitrobenzene was consumed rapidly and aniline formed correspondingly. A notable side-product formanilide was detected after 2 hours, resulting from the condensation of aniline and FA and it was confirmed by a control experiment where aniline was used as initial reactant. To our surprise, no azo or azoxy compounds were detected, suggesting that our reaction system does not strictly follow the Haber's mechanism. In the Haber's mechanism, nitro group is reduced stepwise first to nitrosobenzene and then the hydroxylamine, hydroxylamine can easily react with nitrosobenzene yielding azoxybenzene and then further reduce to azobenzene and eventually aniline, details see Figure S3. However, when nitrosobenzene was employed as reactant in our system, azobenzene was produced predominantly along with the consumption of substrate in the first 5 hours, it was gradually converted to aniline in the rest of reaction period without detection of other intermediates (Figure 3b), and such process is in agreement with Haber's mechanism. Additionally, we received similar result in the reduction of hydroxylamine and azobenzene as shown in Table S3. Thus, we can conclude that the reduction of nitrobenzene directly yield aniline instead of flowing a stepwise reduction process, accordingly a tentative mechanism for the photocatalytic reduction of nitrobenzene is proposed in Figure S4.

Table 3. Isotope abundance of deuterium and 18O in the products of nitrobenzene hydrogenation.

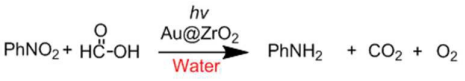

Water = D_2O, $H_2{}^{18}O$

Entry	Water	Conversion (%)	Product	Abundance (%)	
1	D_2O	87		H	D
			$PhNH_2$	34	66
2				^{16}O	^{18}O
	$H_2{}^{18}O$	74	CO_2	63	37
3			O_2	100	0

Reaction conditions: 50 mg Au@ZrO2, 1 mmol nitrobenzene, 2 ml Formic acid mixed with 2 ml water as solvent, light intensity 0.5 W/cm^2, 40 °C, 1 atm Argon, 8 h. The products were identified by mass spectrometry. MS and yields were measured by GC using external standard.

View Article Online
DOI: 10.1039/C7CY02291C

The influence of light wavelength on photocatalysis was studied by investigating action spectra of hydrogenations of styrene, nitrobenzene and benzaldehyde. In an action spectrum, the photocatalytic efficiency is plotted against light wavelength. Quantum yield (Φ) which was converted from reaction rate is used to present the photocatalytic efficiency. It was calculated as followed:

Φ = [the number of converted reactant molecules×100]/[the number of incident photons].

Two types of action spectrum are observed as shown in Figure 4. The result indicates that AuNPs can most efficiently drive the hydrogenation of nitrobenzene by the LSPR effect as the highest Φ value was observed at 530 nm (Figure 4c). For light spectrum other than LSPR wavelength, the photocatalytic activity is attributed to the electrons directly excited by photons.

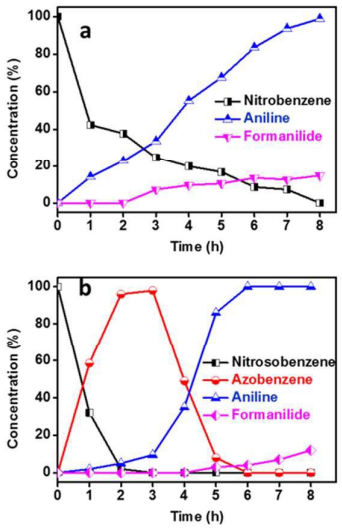

Figure 3. Time-conversion plot. (a) nitrobenzene hydrogenation and (b) nitrosobenzene hydrogenation. Reaction condition: 200 mg Au@ZrO_2 dispersed into a solution of 15 ml of 85% formic acid and 15 ml deionized water, light intensity 0.5 W/cm^2, 40 ℃, 1 atm argon, reaction time 8 h, 0.5 ml specimen was taken every hour and analysed by mass spectrometry (identifying the species) and GC (determining the concentration of the species using external standard).

These photoexcited produced by the photons of shorter wavelength possess higher energy levels but less population. It explains the relatively high quantum yield of 400 nm in hydrogenation of nitrobenzene. The light of 590 nm and 620 nm are neither triggering LSPR effect nor delivering photons with sufficient energy, therefore resulting low reaction rate. In the styrene and benzaldehyde's case (Figure 4a-b), the reaction demands more reduction power, meaning hot-electrons with higher energy, due to their much more negative reduction potential (Table S1). Although strong LSPR absorption can generate a large population of excited electrons,[20] many of them do not have sufficient energy to enable absorbed styrene to cross the activation energy barrier. On the other hand, photons of 400 nm wavelength can generate photoexcited electrons with sufficient energy to drive the reduction of styrene and benzaldehyde. More photoexcited electrons generated by LSPR absorption have sufficient energy to drive the benzaldehyde reduction compared with those in the styrene reduction as the reduction potential of benzaldehyde is higher than that of styrene.

The dependence of the reaction yield on the irradiance was investigated and results are shown in Figure 5, the yield of hydrogenation increases with increasing irradiance for all four reactions. It is direct evidence that irradiation can remarkably promote the hydrogenation reactions. In addition, the relative contribution of the irradiation in comparison to the thermal contribution for the hydrogenation reactions is clarified.

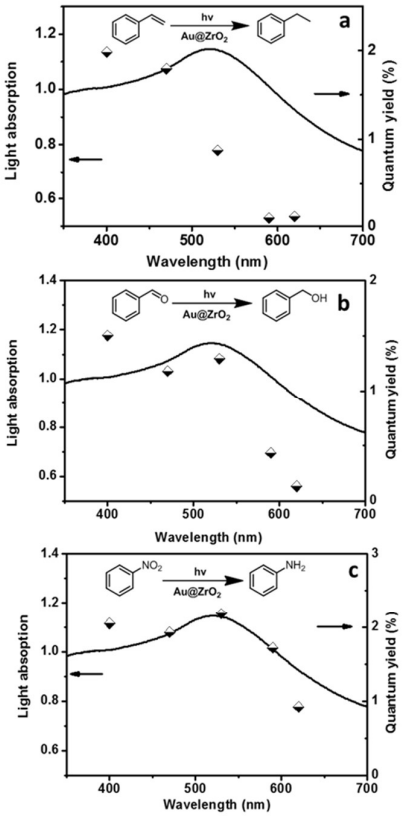

Figure 4. Action spectra of selected hydrogenations. Hydrogenation of styrene (a), benzaldehyde (b) and nitrobenzene (c) catalysed by Au@ZrO_2. The purple line represents the diffuse reflectance UV-vis spectrum of Au@ZrO_2, blue marks represent the quantum yield of each wavelength.

The column is the yield of light reaction while the white part is the yield of the reaction in the dark at the same reaction temperature which represents the contribution of thermal effect. When irradiation was applied, the yield increased significantly and almost linearly. It is also noted that at higher irradiance, the contribution of the irradiation to the overall reaction rate is greater. For example, when the irradiance was 0.1 W/cm^2 the contribution of light to the yield of nitrobenzene hydrogenation was merely 25.6%, while the contribution was 79% when irradiance was raised up to 0.5

View Article Online
DOI: 10.1039/C7CY02291C

W/cm^2. These results indicate that the irradiation is the predominating force driving the hydrogenation reactions. Generally, higher irradiance can produce more photoexcited electrons resulting higher reaction rate. The photoexcited electrons that have insufficient energy to induce the reduction will relax and release their energy to heat the lattice of the AuNP. Such a photo-thermal effect also accelerates the reaction. Therefore, higher reaction rates are always observed at higher irradiance.

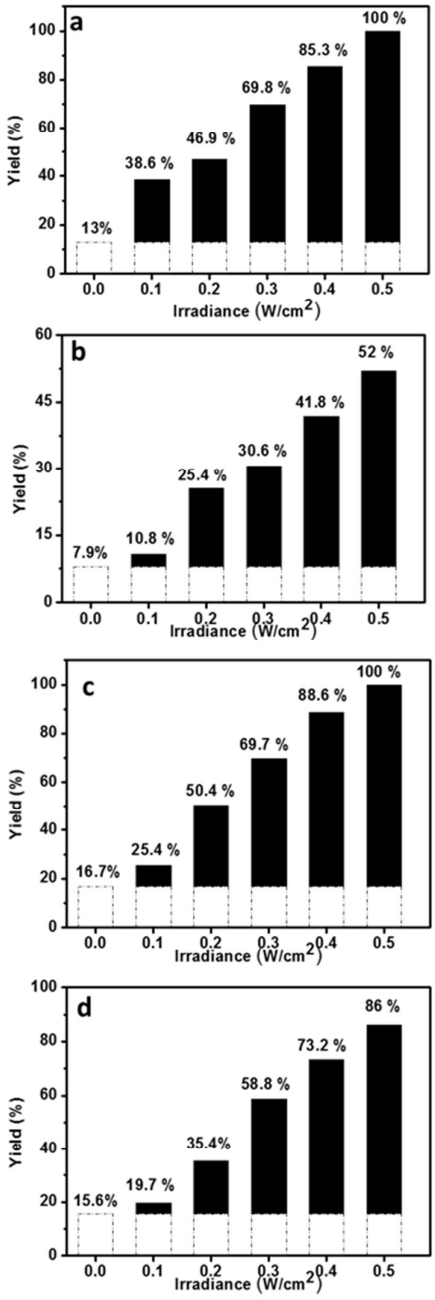

Figure 5. Dependence of the photocatalytic activity of Au@ZrO_2 for hydrogenation on irradiance. The grey part of a column represents the contribution of thermal effect and green column represents the contribution of light. Hydrogenation of nitrobenzene (a), styrene (b), benzyl aldehyde (c) and imine (d).

Lastly, the reusability of the Au@ZrO_2 photocatalyst have been investigated. In the hydrogenation of nitrobenzene, Au@ZrO_2 is recovered by centrifugation after each photocatalytic reaction round, the recovered photocatalyst is washed with water and ethanol and then directly applied in next cycle reaction without further treatment or regeneration. The conversion of nitrobenzene hydrogenation over Au@ZrO_2 remain 97% after six cycle runs as shown in Figure 6. In addition, the TEM images of Au@ZrO_2 after one photocatalytic reaction are collected and shown in Figure S5. The photocatalytic reaction round does not have notable impact on the morphology of Au@ZrO_2. The particle dispersion and size distribution remain unchanged. In addition, surface of sample has not been covered by organics. Thus, the Au@ZrO_2 photocatalyst exhibits good reusability, the reason could be the resistance of Au metal to oxidative and acidic environment, meanwhile the moderate reaction condition is in favour of the reusability of photocatalyst.

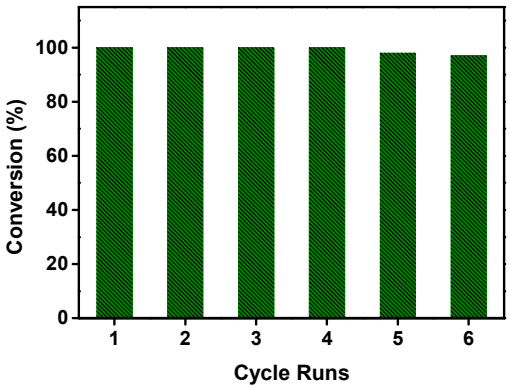

Figure 6. Reusability of Au@ZrO_2 in hydrogenation of nitrobenzene. Reaction conditions: 50 mg Au@ZrO_2 dispersed into a solution of 2 ml of 85% formic acid and 2 ml deionized water containing 0.5 mmol nitrobenzene, light intensity 0.5 W/cm^2, 40 °C, 1 atm argon, reaction time 4 h, specimen was analysed by GC (determining the concentration of the species using external standard).

Conclusions

In summary, this work reports a photocatalytic hydrogenation reaction system for the hydrogenation of five types of unsaturated aromatics using aqueous solutions of FA as the reductive agent over a visible or UV illuminated Au@ZrO_2 photocatalyst at ambient temperatures and pressures. The photocatalytic system exhibits high catalytic efficiency and broad substituent tolerance. One can tune the reduction power of this system over a wide range by regulating the irradiation wavelength, and moderating the reaction temperature. We have found that water plays an active role of enhancing the reductive efficiency of FA, it reacts with FA to yield orthoformic acid that provides the hydrogen to yield H-Au surface species. These H-Au species react with the groups

View Article Online
DOI: 10.1039/C7CY02291C
Journal Name ARTICLE

to be reduced in the hydrogenation. This finding will renew the understanding of the selective reductions and inspire future application of FA as hydrogen source. Another important finding is that the hydrogenation of nitro aromatic compounds follows a mechanism distinct from the well-known Haber mechanism, yielding corresponding anilines directly due to the strong reduction power of the new photocatalytic system. This photocatalytic process is green, in terms of reduction agent, and reaction conditions, is chemoselective, and is feasible for a wide range of molecules.

Experimental Section

Materials. Zirconium(IV) oxide (ZrO_2, particle size <100 nm, TEM), gold (III) chloride trihydrate ($HAuCl_4 \cdot 3H_2O$, ≥99.9% trace metal basis), silver (III) chloride ($Ag(NO_3)_3$, ≥99.9%), sodium borohydride powder ($NaBH_4$, ≥98.0%), Deuterium oxide (D_2O, 99.9 atom% D), Nitrosobenzene (C_6H_5NO, ≥97%), azobenzene ($C_{12}H_{10}N_2$, ≥98%), styrene (C_8H_8, ≥99.9%), N-(phenylmethylene)- Benzenamine ($C_{13}H_{11}N$, ≥96%) and L-lysine (2,6-diaminocaproic acid, ≥97%), were purchased from Sigma-Aldrich (Australia). $H_2{}^{18}O$ (≥96 atom% ^{18}O) was purchased from HuaYi Isotopes Co. (China). Formic acid solution (HCOOH, 85%), ethanol (CH_3OH, ≥95%) and dichloromethane (CH_2Cl_2) were of analytical grade. All chemicals were used as received without further purification unless otherwise noted. The water used in all experiments was prepared by an Ultrapure Water System from Merck Millipore Co.

Synthesis of Au@ZrO_2 photocatalyst. ZrO_2 supported AuNPs (Au@ZrO_2) was prepared by the impregnation-reduction method. For example, to prepare 3 wt% Au@ZrO_2, ZrO_2 powder (2.0 g) was dispersed into an aqueous solution of $HAuCl_4$ (32.7 mL, 0.01 M) under magnetic stirring at room temperature, followed by addition of a lysine aqueous solution (10 mL, 0.53 M) while it was vigorously stirred for 30 min. The pH value of the mixture was 8-9. To this suspension a freshly prepared aqueous $NaBH_4$ (10 mL, 0.35 M) was added dropwise. The mixture was aged overnight, and then the solid was separated by centrifugation, washed with water (three times), ethanol (once), and was dried at 60 °C in a vacuum oven for 24 h.

Characterisation. The morphology and elemental composition of photocatalysts were studied using a JEOL 2100 transmission electron microscopy (TEM) coupled with an energy dispersion X-ray (EDX) spectrometer (X-MAXN 80TLE, OXFORD Instruments). The accelerating voltage of TEM was 200 KV. Diffuse reflectance UV-visible spectra of the catalysts were collected with a Varian Cary 5000 spectrometer with $BaSO_4$ as a reference. The FTIR spectra were measured with a Nicolet 380 instrument.

General procedure for photocatalytic reactions. In a typical activity test, a 25 mL Pyrex round-bottom flask was used as container, and after 1 mmol reactants and 50 mg catalyst had been added, the flask was filled with 1 atm argon gas and sealed in order to isolate the reaction from air. The flask was then stirred magnetically and irradiated with a halogen lamp (from Nelson, 500W, and wavelength in the range of 400-750 nm). The irradiance was 0.5 W/cm^2 unless otherwise specified. The reaction temperature was carefully controlled at 40 ^{o}C by using an air conditioner unless otherwise specified. The reaction system in the dark was conducted using a water bath placed above a magnetic stirrer, and the reaction flask was wrapped with aluminium foil to isolate the contents from the influence of light. The reaction temperature was maintained at the same temperature as the corresponding reaction under irradiation. At the end of reaction time, the product was firstly extracted with equivalent amount of dichloromethane, and then 2 mL aliquots were collected and filtered through a Millipore filter (pore size of 0.45 μm) to remove particulate matter. The clear liquid-phase products were analysed with an Agilent 6980 gas chromatography (GC) using a HP-5 column to analyse the change in the concentrations of reactants and products. An Agilent HP5973 mass spectrometer was used to identify the products. In the analysis of gaseous products, prior to the photocatalytic reaction, the reaction tube was purged with argon gas and sealed to isolate the reaction from air. After reaction, a 1 mL gas sample was taken from the atmosphere above the reaction suspension and analysed using mass spectrometry.

Action Spectrum Test. An action spectrum indicates the dependence of reaction rate on the wavelength of irradiation, which provides evidence for the mechanism of how the photocatalyst responses to different light wavelengths and activates the reactant molecules. Action spectrum experiments were conducted with light emitting diode (LED) lamps (Tongyifang, Shenzhen, China) with wavelengths of 400 ± 5 nm, 470 ± 5 nm, 530 ± 5 nm, 590 ± 5 nm, and 620 ± 5 nm. The light intensity was measured to be 0.50 W/cm2 using an energy meter (CEL-NP2000) from AULTT Company and other reaction conditions were maintained identical to those of typical reaction procedures.

DFT Calculation Methods. Geometry optimization and electronic structure calculations were carried out using density function theory plus long range dispersion correction under the TS method of DFT-D as implemented in the Dmol^3 software[41,42] with Effective Core Potentials. Exchange-correlation interaction is treated as generalized gradient approximation (GGA) with the Perdew, Burke, and Ernzerhof (PBE) functional and electronic Eigen functions are expanded in terms of DND with a real-space cut-off of 4.4 Å. The convergence criteria for energy change, force, and displacement during geometry optimization were set to be 2.0 × 10−5 Ha, 4.0 × 10−3 Ha/Å, and 5.0 × 10−3 Å, respectively. The vacuum space was more than 20 Å, which was enough to avoid the interaction between periodical images.

Conflicts of interest

There are no conflicts to declare.

Acknowledgements

DOI: 10.1039/C7CY02291C

Authors gratefully acknowledge financial support from the Australia Research Council. (DP150102110). The electron microscopy work was performed through a user project supported by the Central Analytical Research Facility (CARF), Queensland University of Technology.

References

1 T. C. Johnson, D. J. Morris, M. Wills, *Chem. Soc. Rev.*, 2010, ***39***, 81-88.
2 U. M. Lindström, *Chem. Rev.*, 2002, ***102***, 2751-2772.
3 S. Narayan, J. Muldoon, M. Finn, V. V. Fokin, H. C. Kolb, K. B. Sharpless, *Angew. Chem. Int. Ed.*, 2005, ***44***, 3275-3279.
4 S. Naskar, M. Bhattacharjee, *Tetrahedron Lett.*, 2007, ***48***, 465-467.
5 A. Fujii, S. Hashiguchi, N. Uematsu, T. Ikariya, R. Noyori, *J. Am. Chem. Soc.*, 1996, ***118***, 2521-2522.
6 G. Wienhöfer, I. Sorribes, A. Boddien, F. Westerhaus, K. Junge, H. Junge, R. Llusar, M. Beller, *J. Am. Chem. Soc.*, 2011, ***133***, 12875-12879.
7 K. Nomura, *J. Mol. Catal. A: Chem.*, 1998, ***130***, 1-28.
8 J. M. Farrell, J. A. Hatnean, D. W. Stephan, *J. Am. Chem. Soc.*, 2012, ***134***, 15728-15731.
9 H. Rogers, *Science*, 1968, ***159***, 1057-1064.
10 G. Zassinovich, G. Mestroni, S. Gladiali, *Chem. Rev.*, 1992, ***92***, 1051-1069.
11 A. Corma, P. Serna, *Science*, 2006, ***313***, 332-334.
12 M. Stein, B. Breit, *Angew. Chem. Int. Ed.* 2013, ***52***, 2231-2234.
13 M.J. Kale, T. Avanesian, H. Xin, J. Yan, P. Christopher, *Nano Lett.*, 2014**,** ***14***, 5405-5412.
14 S. Linic, U. Aslam, C. Boerigter, M. Morabito, *Nat. Mater.*, 2015, ***14***, 567-576.
15 Y. Duan, L. Li, M.-W. Chen, C.-B. Yu, H.-J. Fan, Y.-G. Zhou, *J. Am. Chem. Soc.*, 2014, ***136***, 7688-7700.
16 P. Zhao, X. Feng, D. Huang, G. Yang, D. Astruc, *Coord. Chem. Rev.*, 2015, ***287***, 114-136.
17 X. Guo, C. Hao, G. Jin, H.-Y. Zhu, X.-Y. Guo, *Angew. Chem. Int. Ed.*, 2015, ***53***, 1973-1977.
18 X. Chen, H.-Y. Zhu, J.-C. Zhao, Z.-F. Zheng, X.-P. Gao, *Angew. Chem. Int. Ed.,* 2008, ***47***, 5353-5356.
19 H. Zhu, X. Ke, X. Yang, S. Sarina, H. Liu, *Angew. Chem. Int. Ed.*, 2010, ***49***, 9657-9661.
20 S. Linic, P. Christopher, D. B. Ingram, *Nat. Mater.*, 2011, ***10***, 911-921.
21 S. Linic, U. Aslam, C. Boerigter, M. Morabito, *Nat. Mater.*, 2015, ***14***, 567-576.
22 L. Zhou, C. Zhang, M.J. McClain, A. Manjavacas, C.M. Krauter, S. Tian, F. Berg, H.O. Everitt, E.A. Carter, P. Nordlander, N.J. Halas, *Nano Lett.*, 2016, ***16***, 1478-1484.
23 L. Brus, *Acc. Chem. Res.*, 2008, ***41***, 1742-1749.
24 J.G. Smith, J.A. Faucheaux, P.K. Jain, *Nano Today*, 2015, ***10***, 67-80.
25 Q. Xiao, E. Jaatinen, H. Zhu, *Chem. Asian J*. 2014, ***9***, 3046-3064.
26 Z. Liu, Y. Huang, Q. Xiao, H. Zhu, *Green Chem.*, 2016, ***18***, 817-825.
27 M. Wen, Y. Kuwahara, K. Mori, H. Yamashita, *Top. Catal.*, 2016, ***59***, 1765-1771.
28 M. Garcia, *J. Phys. D: Appl. Phys.*, 2011, ***44***, 283001-283021.
29 S. Sarina, H. Zhu, Q. Xiao, E. Jaatinen, J. Jia, Y. Huang, Z. Zheng, H. Wu, *Angew. Chem. Int. Ed.*, 2014, ***53***, 2935-2940.
30 S. Peiris, J. McMurtrie, H.-Y. Zhu, *Catal. Sci. Technol.*, 2016, ***6***, 320-338.
31 P. Christopher, H. Xin, A. Marimuthu, S. Linic, Nat. *Mater.*, 2012, ***11***, 1044-1050.
32 M.-C. Fu, R. Shang, W.-M. Cheng, Y. Fu, *Angew. Chem. Int. Ed.*, 2015, ***54***, 9042-9046.
33 X. Ke, S. Sarina, J. Zhao, X. Zhang, J. Chang, H. Zhu, *Chem. Commun.*, 2012, ***48***, 3509-3511.
34 S.-J. Lai, D. Yang, Y.-Q. Li, X.-L. Zhao, Y. Lu, Y. Liu, *Eur. J. Inorg. Chem.*, 2015, ***2015***, 1408-1416.
35 L. Yu, Q. Zhang, S.-S. Li, J. Huang, Y.-M. Liu, H.-Y. He, Y. Cao, *ChemSusChem*, 2015, ***8***, 3029-3035.
36 M. D. Pluth, R. G. Bergman, K. N. Raymond, *J. Am. Chem. Soc.*, 2008, ***130***, 11423-11429.
37 A. Abad, P. Concepción, A. Corma, H. García, *Angew. Chem. Int. Ed.*, 2005, ***44***, 4066-4069.
38 P. Lucio Anelli, C. Biffi, F. Montanari, S. Quici, *J. Org. Chem.*, 1987, ***52***, 2559-2562.
39 X. Zhao, Y. Zhao, G. Fu, N. Zheng, *Chem. Commun.*, 2015, ***51***, 12016-12019.
40 P. Roth, J. C. Yoder, T.-J. Won, J. M. Mayer, *Science*, 2001, ***294***, 2524-2526.
41 B. Delley, *J. Chem. Phys.,* 1990, ***92***, 508-517.
42 B. Delley, *J. Chem. Phys*., 2000, ***113***, 7756-7764.